# Transmembrane Peptides Stabilize Inverted Cubic Phases in a Biphasic Length-Dependent Manner: Implications for Protein-Induced Membrane Fusion

D. P. Siegel,* V. Cherezov,† D. V. Greathouse,‡ R. E. Koeppe II,‡ J. Antoinette Killian,§ and M. Caffrey†¶**
*Givaudan Inc., Cincinnati, Ohio; †Department of Chemistry, The Ohio State University, Columbus, Ohio; ‡Department of Chemistry and Biochemistry, University of Arkansas, Fayetteville, Arkansas; §Department of Biochemistry of Membranes, University of Utrecht, Utrecht, The Netherlands; ¶Biochemistry and Biophysics Programs, The Ohio State University, Columbus, Ohio; and **College of Science, University of Limerick, Limerick, Ireland

ABSTRACT WALP peptides consist of repeating alanine-leucine sequences of different lengths, flanked with tryptophan "anchors" at each end. They form membrane-spanning $\alpha$-helices in lipid membranes, and mimic protein transmembrane domains. WALP peptides of increasing length, from 19 to 31 amino acids, were incorporated into *N*-monomethylated dioleoylphosphatidylethanolamine (DOPE-Me) at concentrations up to 0.5 mol % peptide. When pure DOPE-Me is heated slowly, the lamellar liquid crystalline ($L_\alpha$) phase first forms an inverted cubic ($Q_{II}$) phase, and the inverted hexagonal ($H_{II}$) phase at higher temperatures. Using time-resolved x-ray diffraction and slow temperature scans (1.5°C/h), WALP peptides were shown to decrease the temperatures of $Q_{II}$ and $H_{II}$ phase formation ($T_Q$ and $T_H$, respectively) as a function of peptide concentration. The shortest and longest peptides reduced $T_Q$ the most, whereas intermediate lengths had weaker effects. These findings are relevant to membrane fusion because the first step in the $L_\alpha/Q_{II}$ phase transition is believed to be the formation of fusion pores between pure lipid membranes. These results imply that physiologically relevant concentrations of these peptides could increase the susceptibility of biomembrane lipids to fusion through an effect on lipid phase behavior, and may explain one role of the membrane-spanning domains in the proteins that mediate membrane fusion.

## INTRODUCTION

WALP peptides are hydrophobic, $\alpha$-helical transmembrane peptides that incorporate into lipid bilayers (1–5). The helical axes of such peptides are nearly perpendicular to the plane of the membrane at room temperature (1,3,4,6–8) and the core of the helices, when membrane-embedded, is strongly protected from solvent deuterium exchange (9). Because of these properties, WALP peptides are models for the single helical membrane-spanning domains found in some integral membrane proteins (1,4). WALP peptides stabilize inverted phases in phospholipids in a peptide-length- and concentration-dependent fashion. In previous studies, peptides whose lengths as rigid $\alpha$-helices are short compared to the thickness of the lamellar phase bilayer of the host lipid were generally found to be effective in inducing nonlamellar phase formation, with the concentration required depending on the nature of the lipids. For example, it was shown that high concentrations of short WALP peptides (~10 mol %) can induce formation of $H_{II}$ and so-called isotropic phases in fully hydrated phosphatidylcholine systems (1–3), which only form the lamellar liquid crystalline ($L_\alpha$) phase in the absence of the peptides. Peptide concentrations of 1–4 mol % can substantially lower the $L_\alpha/H_{II}$ transition temperature and induce formation of an inverted cubic ($Q_{II}$) phase in 1,2-dielaidoyl-*sn*-3-glycero-3-phosphoethanolamine (DEPE) (10). WALP concentrations as small as 0.1 mol % substantially lowered the temperature for isotropic phase formation in a 1,2-dioleoyl-*sn*-glycero-3-phosphoethanolamine/1,2-dioleoyl-*sn*-glycero-3-phosphoglycerol (DOPE/DOPG) mixture (11). Also, in previous studies, WALP peptides with lengths longer than the host lipid bilayer thickness were found to have little or no effect (10,11) on the phase behavior of the lipids. The fact that WALP peptides and other transmembrane peptides (12) can stabilize nonlamellar ($H_{II}$ and $Q_{II}$) phases is especially interesting in light of the association of inverted phase behavior with membrane fusion (see, e.g., Ellens et al. (13) and Siegel (14)) and the possible influence of inverted phase behavior on membrane protein function (reviewed in Epand (15)).

This work deals with the influence of WALP peptides on the formation of $Q_{II}$ and $H_{II}$ phases from the $L_\alpha$ phase in DOPE-Me. These experiments were motivated by an interest in the physical chemical mechanisms by which proteins induce biomembrane fusion, which are still poorly understood. There is a close relationship between $Q_{II}$ phase formation and the occurrence of membrane fusion in some pure lipid systems. Simply stated, formation of membrane fusion pores is postulated to be the first step in the $L_\alpha/Q_{II}$ phase transition (14,16). Membrane fusion rates increase substantially as unilamellar vesicle dispersions of DOPE-Me and DOPE/1,2-dioleoyl-*sn*-glycero-3-phosphocholine lipid mixtures are incubated at increasing temperatures in the region where $Q_{II}$ phase precursors and $Q_{II}$ phases are detected by $^{31}$P NMR and freeze-fracture electron microscopy

*Submitted July 11, 2005, and accepted for publication September 13, 2005.*

Address reprint requests to David P. Siegel, Givaudan Inc., 1199 Edison Drive, Cincinnati, OH 45215. Tel.: 513-948-4840; E-mail: david.siegel@givaudan.com.



0006-3495/06/01/200/12 $2.00
doi: 10.1529/biophysj.105.070466

(13). The $Q_{II}$ precursors are catenoidal connections (interlamellar attachments) with central water channels that form between lamellae (17–19). These connections, formed between unilamellar liposomes, would achieve fusion between the liposomes (nonleaky continuity of both the liposomal membranes and aqueous contents). Siegel et al. (17,18) showed that the connections formed in unilamellar liposomal dispersions in the same temperature region as the observed increases in membrane fusion rates (13), and that they formed lattices closely resembling the lattices of catenoidal intermediates proposed earlier (20) as precursors to $Q_{II}$ phase formation (21). Thus, one can study physical chemical influences on the fusion rate in model membrane systems by determining whether given changes in composition or conditions alter the onset temperature for the $L_\alpha/Q_{II}$ phase transition ($T_Q$). A number of authors have exploited this relationship in studying the effects of small peptides and lipid additives on membrane fusion in DOPE-Me (see, e.g., Yeagle et al. (22), Epand and Epand (23), Epand et al. (24), Nieva et al. (25), Davies et al. (26), and Basáñez et al. (27)). DOPE-Me is an appropriate choice of lipid for such studies because, at slow temperature scan rates (e.g., 1.5°C/h), it has a well characterized $L_\alpha/Q_{II}$ phase transition that begins at ~59.6°C (28).

There is increasing evidence that membrane-spanning domains are important for activity of proteins that mediate membrane fusion (reviewed in Schroth-Diez et al. (29)). Moreover, peptides corresponding to the membrane-spanning domains of these proteins fuse liposomes in the absence of other peptides or proteins (30–33). The only domains of the fusion-mediating protein in influenza virus that have been demonstrated to closely associate with the lipids of target and host membrane lipids under fusogenic conditions are the so-called fusion peptides and the membrane-spanning domains of the same protein (34). The interactions of fusion peptides with lipids have been studied extensively for almost two decades (35) (for reviews, see Nieva and Agirre (36), Tamm et al. (37,38), and Martin et al. (39)), whereas biophysical characterization of the membrane-spanning domains of fusion proteins and their activity in liposome fusion started more recently (30–33,40).

In this study, we used time-resolved x-ray diffraction (TRXRD (41)) to determine the changes in lipid phase behavior (and especially changes in $T_Q$) induced by adding WALP peptides to DOPE-Me. By using TRXRD and a host lipid with a well defined $T_Q$ (28), we can determine the effects of different peptides on $Q_{II}$ phase formation with greater precision than in previous studies (see, e.g., van der Wel et al. (10), Morein et al. (11), and Liu et al. (12)). Also, TRXRD directly verifies the presence of $Q_{II}$ phases, whereas other methods, such as $^{31}P$ NMR, cannot distinguish between $Q_{II}$ phases and $Q_{II}$ phase precursors. In light of recent theoretical work (16), the results allow us to estimate the effects that such membrane-spanning peptides have on the stability of fusion pores. It can be shown (16) that 1 mol % of a particular WALP peptide would lower the energy of fusion pores in a lipid such as DOPE-Me by as much as 40 $k_BT$.

## MATERIALS AND METHODS

### Materials

#### *Buffers and reagents*

Buffers and reagents were as described in Cherezov et al. (28).

#### *WALP peptide synthesis*

Table 1 shows the sequences of the peptides used in this study. The peptides were prepared by fluorenylmethoxycarbonyl (Fmoc) solid-phase methods on an ABI 433A peptide synthesizer (PE Biosystems, Foster City, CA). The Fmoc amino acids, from Advanced ChemTech (Louisville, KY) or Bachem Bioscience (King of Prussia, PA), were coupled as hydroxybenzotriazol esters in the presence of [2-(1 *H*-benzotriazol-1-yl)-1,1,2,3-tetramethyluronium hexafluorophosphate] to a preloaded Fmoc-L-Ala Wang resin (Advanced ChemTech). All peptide synthesizer reagents were purchased from PE Biosystems except dichloromethane and *N*-methylpyrrolidinone, which were high-performance liquid chromatography (HPLC)-grade obtained from Allied Signal (Muskegon, MI). Occasional failure sequences, due to incomplete coupling of a particular hydrophobic amino acid, were capped using acetic anhydride; this precaution was important to prevent the accumulation of significant amounts of (n-1) or (n-2) peptides. Fmoc-deprotection at each step was with piperidine/*N*-methylpyrrolidinone (1:4 v/v). The synthesis was completed by coupling acetyl-Gly (Advanced ChemTech), also as the hydroxybenzotriazol ester. The completed peptides were cleaved from the resin with 20 vol % distilled ethanolamine (Aldrich Chemical, Milwaukee, WI) in dichloromethane for 48 h at 25°C (42). The peptides were lyophilized to a white powder from trifluoroethanol (TFE)/water (1:1 v/v). Based on analytical HPLC, the purity of the peptides was 80–95%.

Some batches of WALP 19, 23, 27, and 31 were further purified via reversed-phase HPLC. These will be referred to as purified peptides. Samples of WALP19, WALP23, and WALP27 were dissolved in TFE (50 mg/mL) and purified on a Zorbax SB-C8 semipreparative column using a solvent gradient of methanol and 0.1 vol % trifluoracetic acid in deionized water. After purification, the peptides were lyophilized to a white powder from TFE/deionized water (50:50 v/v) as described above, and their purity was estimated to be 98% by analytical reversed-phase HPLC analysis and electrospray mass spectral analysis. Due to its length, WALP31 was HPLC-purified using a Nucleosil column (SI 100-10, pore size 100 Å), obtained from Macherey-Nagel (Düren, Germany) with chloroform/methanol/water (80:19:1 v/v) as eluent, and then lyophilized to a white powder, ~98% pure. HPLC purification of these very hydrophobic peptides results in a large peptide loss, presumably because of aggregate formation.

**TABLE 1 Sequences and lengths of the WALP peptides used**

| Peptide | Sequence | Length as an $\alpha$-helix (Å)* |
|---|---|---|
| WALP19 | Ac-GWW-$(LA)_6$ L-WWA-e | 28.5 |
| WALP23 | Ac-GWW-$(LA)_8$ L-WWA-e | 34.5 |
| WALP25 | Ac-GWW-$(LA)_9$ L-WWA-e | 37.5 |
| WALP27 | Ac-GWW-$(LA)_{10}$ L-WWA-e | 40.5 |
| WALP31 | Ac-GWW-$(LA)_{12}$ L-WWA-e | 46.5 |

Ac, acetyl; e, ethanolamine; A, alanine; G, glycine; L, leucine; and W, tryptophan.

*The helix length was calculated by multiplying the number of residues by 1.5 Å.

### DOPE-Me

*N*-monomethylated 1,2-dioleoyl-*sn*-glycero-3-phosphoethanolamine (DOPE-Me) was used as received from Avanti Polar Lipids (Alabaster, AL), as lyophilized powder. All the DOPE-Me used in this study was from the same lot that was used in studies of the $L_\alpha/Q_{II}$ transition in pure DOPE-Me (28). Lipid received from the manufacturer was stored at −70°C until samples were prepared for x-ray diffraction experiments.

## Methods

### DOPE-Me/peptide samples

Peptides were mixed with DOPE-Me using a TFE/water lyophilization technique developed previously (1). WALP peptide stock solutions (0.3–3.4 mg/mL, depending on the peptide and the desired concentration in the lipid) were made up in TFE. The WALP peptide concentration in the TFE stock solution was determined by the absorbance after dilution with methanol (final methanol concentration >95% v/v) at 280 nm, using blank solutions of the same TFE/methanol ratio. The molar extinction coefficient of *N*-tertiary butyloxycarbonyl L-tryptophan at 280 nm was determined in methanol as 5590 $M^{-1}$ $cm^{-1}$ (data not shown). Since there are four tryptophan residues in each WALP peptide, we used a molar extinction coefficient of 22,400 $M^{-1}$ $cm^{-1}$ for all the peptides. An appropriate amount of lyophilized DOPE-Me as received from the supplier was weighed into a Pyrex flask and hydrated with 0.25 mL of Milli-Q water by vortex mixing. A 0.25-mL of WALP peptide stock solution of appropriate concentration in TFE was added to the hydrated DOPE-Me with vortex mixing, diluted with 3.75 mL of water with vortex mixing on ice, frozen in liquid nitrogen, and then lyophilized. Lyophilized samples were hydrated in 150 mM NaCl, 20 mM *N*-tris[Hydroxymethyl]methyl-2-aminoethane-sulfonic acid, 0.1 mM EDTA, pH 7.4, by vortex mixing under Ar and equilibrating on ice for 1 h, after which they were subjected to six freeze/thaw cycles (dry ice/room temperature water). Peptide concentrations are given in units of mol % (100 × moles of peptide/(moles of peptide + moles of DOPE-Me)). The error in peptide concentration in each sample is estimated to be ±5%.

### X-ray diffraction samples

Samples were prepared as described previously (28). Capillaries were stored in closed, screw-capped test tubes at −70°C until they were used (generally less than two weeks). Values of $T_Q$ obtained on single sets of samples observed after different times of storage at −70°C were the same to within the reproducibility of the measurement (1°C) for samples stored for at least 35 days. Values of $T_Q$ determined by rotating anode x-ray diffraction experiments with samples made using different preparations of the same WALP peptide were the same to within 2°C after storage times of 1–35 days.

### Rotating anode and synchrotron source x-ray diffraction measurements

These measurements were performed using the same apparatus and methods described in detail in (28), with the following exceptions. In the synchrotron-source experiments, a monochromatic x-ray beam of either 8.979 keV (wavelength 1.38 Å) or 8.045 keV (wavelength 1.54 Å) was focused at a detector position of 125.5 cm (8.979 keV) or 112.0 cm (8.045 keV), as was determined using a silver behenate standard (43). The temperature in the sample cell was determined using thermocouples inserted into sample capillaries, and was correct to within 0.2°C versus NBS-traceable standards (28). Samples were incubated for 1 h at the starting temperature before any of the experiments commenced. During temperature-scan experiments diffraction patterns were collected using 1-min exposures and at 8-min intervals, at a scan rate of 1.5°C/h. These correspond to intervals of 0.2°C, and to changes in temperature of 0.025°C during each exposure. One data set (0.5 mol % WALP27 in DOPE-Me) was obtained at a scan rate of 2°C/h, with 1-min exposures every 7.5 min (exposures at intervals of 0.25°C). All temperature-scan experiments were performed in the heating direction. The temperature range examined for all peptides extended to 12°C above $T_Q$. In temperature-jump experiments, twenty 1-min exposures were collected in succession, followed by eight 1-min exposures at intervals of 5 min and three or more 1-min exposures at intervals of 10 min. The x-ray shutter was closed during the idle time between exposures to minimize radiation damage (28,44,45).

### Radiation damage study

A radiation damage study protocol very similar to that described for experiments with pure DOPE-Me (28) was followed. Using NSLS beamline X-12B (8.979 keV), we exposed a capillary containing 0.5 mol % WALP31 in DOPE-Me continuously for 1 h at 35°C. This temperature is ~3°C below the temperature at which $Q_{II}$ phases first formed from the $L_\alpha$ phase in a sample of the same preparation, as determined from a previous rotating anode temperature-scan experiment. As with the sample of pure DOPE-Me treated in the same way at 57°C (28), 60 successive 1-min exposures were made while the sample was in the x-ray beam, and patterns obtained during this time showed the presence of only lamellar phase. Immediately after the 60-min irradiation, 1-min exposures were used to collect diffraction patterns from adjacent, unirradiated regions of the same sample. As with the pure DOPE-Me sample (28), the intensity of the lamellar phase diffraction peaks decreased with time throughout the irradiation, and decreased slightly in the displaced patterns (obtained 12–20 min after the end of the experiment) versus the final pattern obtained during the 60-min irradiation. As discussed in Cherezov et al. (28), this continuous decrease also occurs in DOPE-Me samples irradiated only intermittently and DOPE-Me samples examined with much weaker rotating-anode x-ray sources (see, e.g., Gruner et al. (46)). Since the $Q_{II}$ phase was not observed in the 0.5 mol % WALP31 sample irradiated for 60 min, we conclude that the radiation doses used in these experiments had no effect or very minor effects on the observed transition temperatures and lipid phase behavior.

## RESULTS

### TRXRD experiments

Previously, we showed that, when heated at a scan rate of 1.5°C/h, DOPE-Me forms a $Q_{II}$ phase starting at 59.6 ± 0.6°C, and then the $H_{II}$ phase (to coexist with the $Q_{II}$ phase) starting at 63.7 ± 0.4°C (28). The inclusion of WALP peptides alters these temperatures. An example of synchrotron TRXRD data is given in Fig. 1, which shows a diffraction pattern obtained with 0.2 mol % WALP19 in DOPE-Me at 53°C. It was collected as part of a series as the sample was heated from 44.7 to 54.9°C at 1.5°C/h. This pattern was chosen because it shows the simultaneous presence of diffraction rings from the $Q_{II}$-Pn3m, $H_{II}$, and $L_\alpha$ phases during a series of phase transitions from the lamellar phase. WALP-containing samples were examined using slow temperature scans because the $L_\alpha/Q_{II}$ phase transition in pure DOPE-Me is very slow (hours) and hysteretic (21,28). A direct $L_\alpha/Q_{II}$ phase transition is detected in pure DOPE-Me only when the temperature scan rate is <3°C/h, and the observed transition temperature is nearly constant with decreasing scan rate at ≤1.5°C/h (28). Therefore, we used a scan rate of 1.5°C/h in our rotating-anode and

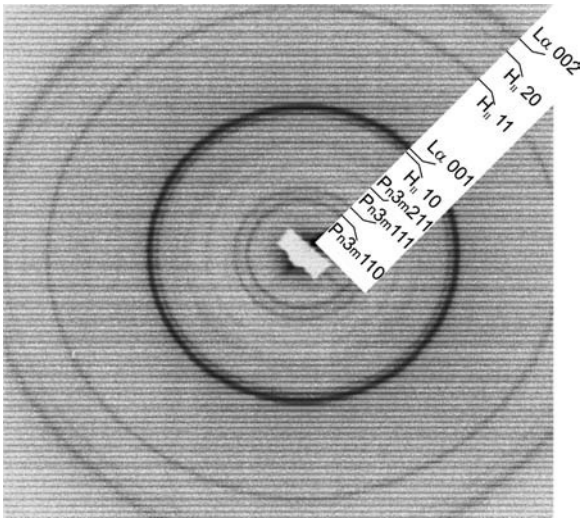


FIGURE 1 Typical two-dimensional detector image of a diffraction pattern from 0.2 mol % WALP19 in DOPE-Me at 53°C recorded using synchrotron radiation. This pattern was obtained in a 1-min exposure as described in Cherezov et al. (28), as part of a series as the sample was heated from 44.7°C to 54.9°C at a scan rate of 1.5°C/h. This pattern shows the presence of diffraction rings from $Q_{II}$-(Pn3m), $H_{II}$, and $L_\alpha$ phases, as labeled in the figure. The $Q_{II}$-Pn3m (110) reflection and $L_\alpha$ (002) reflections are at 174 Å and 31.1 Å, respectively.

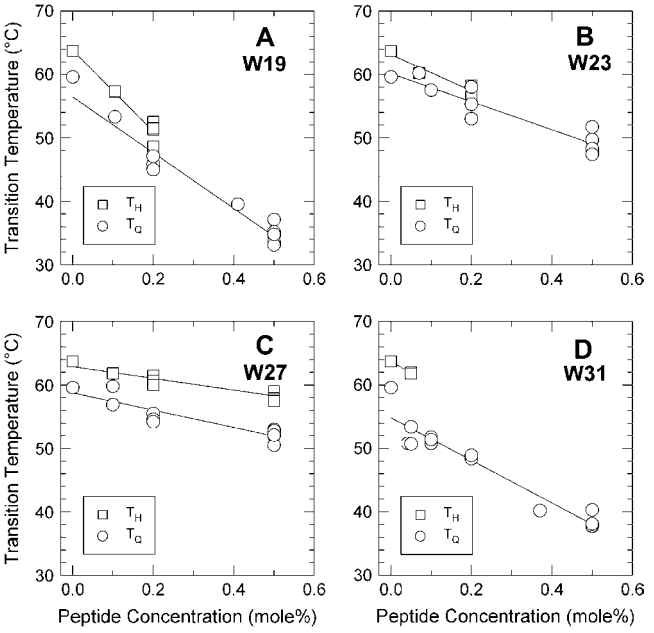


FIGURE 2 Effects of WALP peptides on the onset temperatures for formation of $Q_{II}$ ($T_Q$) and $H_{II}$ phases ($T_H$) in DOPE-Me as a function of peptide length and concentration, as determined via rotating-anode TRXRD experiments. The lines in the plots are linear regression fits to the data. The correlation coefficients for the plots of $T_Q$ and $T_H$, respectively, are (*A*) 0.954 and 0.944; (*B*) 0.887 and 0.911; (*C*) 0.791 and 0.883; and (*D*) 0.925 and 0.991. The fits included the data at zero concentration. The $T_Q$ value at zero peptide concentration (59.6 ± 0.6°C; pure DOPE-Me) represented six measurements. In the case of WALP31, the intercept of the $T_Q$ line with the temperature axis is 4.8°C below $T_Q$ for pure DOPE-Me.

synchrotron experiments to avoid possible ambiguities in phase behavior. Formally, for the $Q_{II}$ phases noted as $Q_{II}$-Pn3m in this work, we cannot distinguish between the space groups Pn3m and Pn3 (47). Harper et al. state that these cannot be distinguished on the basis of powder patterns alone (48).

## Transition temperatures as determined by TRXRD experiments

$T_Q$ and $T_H$ are the onset temperatures for formation of the $Q_{II}$ and $H_{II}$ phases, respectively. Lamellar and nonlamellar phases coexisted over temperature intervals of between 3° and 10°. Fig. 2 summarizes the rotating-anode TRXRD transition temperature data on WALP/DOPE-Me systems. The plots in Fig. 2 show the dependence of $T_Q$ and $T_H$ on the concentration of WALP peptide for four peptides: WALP19, WALP23, WALP27, and WALP31. As for pure DOPE-Me (28), $T_Q$ was determined as the temperature at which the first low-angle reflections (corresponding to spacings of ~220 Å) appeared. The presence of $Q_{II}$ phases under these conditions was verified by synchrotron source temperature scan-experiments, which will be discussed below. For different capillaries made from the same WALP/DOPE-Me sample, the reproducibility of $T_Q$ as determined from rotating anode streak-camera images was generally to within ±1°C. For capillaries made from different samples of the same WALP peptide, the reproducibility was ±2.5°C or less. Therefore different samples of the same peptide had the same efficacy in lowering $T_Q$ to within the error of the measurements.

The data in Fig. 2 show that all the WALP peptides lower $T_Q$ and $T_H$, which for the pure lipid under these conditions are 59.6 ± 0.6°C and 63.7 ± 0.4°C, respectively (28). Both $T_Q$ and $T_H$ decrease linearly with increasing peptide concentration over most of the concentration range. The extent of the effects on $T_Q$ and $T_H$ depends on the length of the WALP peptide.

The slopes of the plots of $T_Q$ versus peptide concentration are −45°C/mol %, −22°C/mol %, −13°C/mol %, and −34°C/mol % for WALP19, WALP23, WALP27, and WALP31, respectively. This shows that the shortest (WALP19) and longest (WALP31) peptides are most effective in reducing $T_Q$, whereas the intermediate-length peptides have more modest effects. Measurements of $T_Q$ were also made for samples containing 0.5 mol % of the peptide WALP25. From these measurements, a value of $T_Q$ of 53.6 ± 1.3°C (average of four determinations) was determined. The peptide-length-dependent effects on $T_Q$ evaluated at 0.5-mol % peptide concentration are summarized in Fig. 3. The data for the pure hydrated DOPE-Me represents the average of six trials (59.6°C ± 0.6°C).

In control experiments using 0.5 mol % of purified WALP19, WALP23, WALP27, and WALP31 (Fig. 3), the purified peptides (*open circles*) lowered the $T_Q$ of DOPE-Me

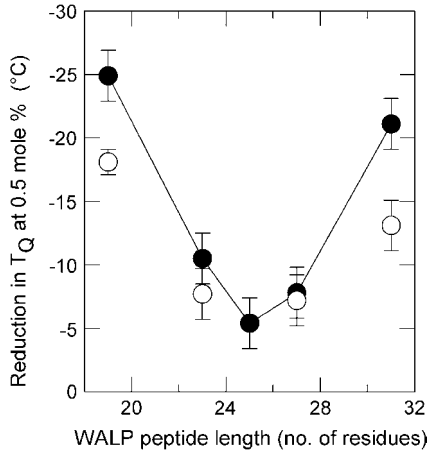


FIGURE 3 Summary of the effects of WALP peptides on $T_Q$ as a function of WALP peptide sequence length. The plot shows the extent of reduction in $T_Q$ at a peptide concentration of 0.5 mol % for each WALP peptide examined in this study. The data are plotted in this fashion to facilitate comparison of the purified WALP peptides and WALP25, which were studied only at a concentration of 0.5 mol %, with the data for the peptides in Fig. 2. (●) Nonpurified peptides. (○) Purified peptides.

with qualitatively similar length dependence as the nonpurified peptides (*solid circles*). However, the extent of reduction in $T_Q$ for each WALP length was smaller for the purified peptides, in particular for the shortest and longest peptides.

The effects of the peptides on $T_H$ were rather similar to those on $T_Q$. The slopes of the plots of $T_H$ versus peptide concentration are −64°C/mol %, −29°C/mol %, −8°C/mol %, and −36°C/mol % for WALP19, WALP23, WALP27, and WALP31, respectively, showing that the shortest (WALP19) and longest (WALP31) peptides are most effective in reducing $T_H$. For samples containing 0.5 mol % of WALP25, $T_H$ was found to be 58.2 ± 0.3°C. Thus, WALP25 only has a small effect on $T_H$, rather similar to that of WALP27.

At relatively high peptide concentrations of 0.5 mol %, $H_{II}$ phases were observed only for WALP27 and WALP25, at ~5°C above $T_Q$ (Fig. 2 *C*). Pure DOPE-Me forms the $H_{II}$ phase at ~4°C above $T_Q$ when examined in similar slow temperature-scan heating experiments. Thus, WALP25 and WALP27 perturb the phase behavior of DOPE-Me less than the other WALP peptides.

Synchrotron source temperature-scan experiments were performed on eight of the WALP/DOPE-Me compositions, to refine the measurements of $T_Q$, determine which $Q_{II}$ phases formed, and study the behavior of the $Q_{II}$ phase lattice constants with temperature and time after temperature jumps. An example of the synchrotron TRXRD data on $Q_{II}$ phase formation is shown in Fig. 4 *A*, for 0.5 mol % WALP31 in DOPE-Me. In this experiment, the sample was heated continuously from 35.0°C to 39.0°C, at 1.5°C/h. The only peaks in the 35.0°C pattern correspond to the first- and

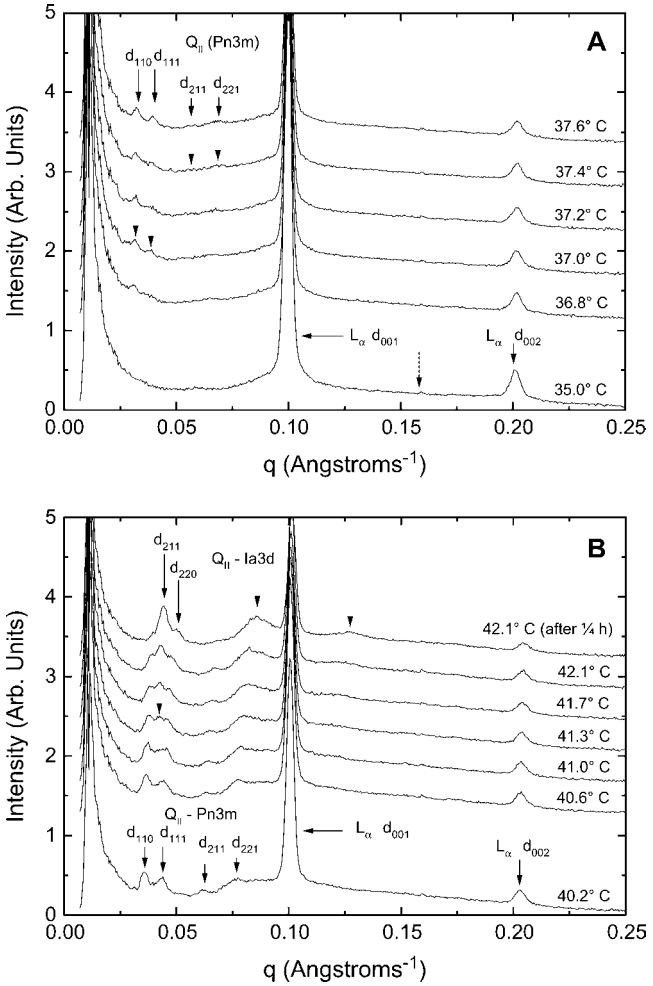


FIGURE 4 Results of synchrotron temperature-scan experiments using 0.5 mol % WALP31 in DOPE-Me, showing formation of $Q_{II}$ phases. The curves are the radial integrals of two-dimensional diffraction patterns like the one in Fig. 1, taken at temperature intervals of 0.2°C. The ordinate is the diffracted intensity, and the abcissa is the magnitude of the scattering vector $q = 2\pi/d$, where $d$ is the interplane spacing in Å. (*A*) Diffraction patterns from an experiment in which the temperature was increased continuously at 1.5°C/h, from 35.0°C to 39.0°C. The only peaks in the 35.0°C pattern are the indicated reflections from the $L_\alpha$ phase. At 37.0°C, two peaks appear at $q = \sim 0.032$ and 0.038 Å$^{-1}$ (*arrowheads*). At 37.4°C, two more small peaks appear at ~0.057 Å$^{-1}$ and 0.069 Å$^{-1}$ (*arrowheads*). In the pattern at 37.6°C, the four new peaks are labeled as the indicated reflections from a $Q_{II}$-Pn3m phase. (*B*) Diffraction patterns obtained from another sample of 0.5 mol % WALP31 in DOPE-Me, heated at 1.5°C/h between 37.0°C and 42.1°C. The pattern at 40.2°C shows the same $Q_{II}$-Pn3m and $L_\alpha$ phase reflections as the 37.6°C pattern in *A*. A new peak at $q = 0.042$ Å$^{-1}$ became clearly visible in the 41.3°C data (*arrowhead*). In the pattern at 42.1°C, this peak had grown in intensity at the expense of the $Q_{II}$-Pn3m reflections. The plot at the top of the figure was obtained 15 min after the end of the scan, with the temperature constant at 42.1°C. Additional peaks are visible in this pattern (*arrowheads*). The two peaks indicated by arrows index as the first two (211 and 220) reflections of a $Q_{II}$-Ia3d phase. The higher-$q$ peaks likely correspond to the superposition of multiple reflections, and could not be reliably indexed. Dashed arrow in *A*: the very small feature in the baseline at $q = 0.159$ Å$^{-1}$ is due to a flaw in the detector, and does not represent a diffraction peak.

second-order reflections from the $L_\alpha$ phase, at $q = 0.100$ Å$^{-1}$ and 0.201 Å$^{-1}$ (62.8 and 31.3 Å), respectively. At 36.8°C, a broad peak appeared at $q = 0.028$–$0.04$ Å$^{-1}$. This resolved into two peaks at $q = \sim 0.032$ Å$^{-1}$ and 0.038 Å$^{-1}$ ($d = \sim 196$ and 165 Å) at 37.0°C (Fig. 4 *A*, *arrowheads*). These two peaks are at $q$ values in approximately the correct ratio to correspond to the 110 and 111 reflections from a $Q_{II}$-Pn3m lattice. At 37.6°C, two additional broad peaks became discernible at $q = \sim 0.057$ Å$^{-1}$ and 0.069 Å$^{-1}$ ($d = \sim 110$ and 91 Å). Although of low intensity, these two peaks persisted up to the end of the scan at 39.0°C (data not shown). The same two peaks were also observed in a second temperature scan on a sample of the same composition (Fig. 4 *B*; see below) starting at 38.0°C (data not shown). The set of four peaks visible at 37.6°C index as the 110, 111, 211, and 221 reflections from a $Q_{II}$-Pn3m phase. To the eye, this series is missing the 200 and 220 reflections, but these are usually weak in diffraction patterns from $Q_{II}$ phases of DOPE-Me (21,28). Peak-fitting procedures identified the weak $d_{220}$ reflection. These five reflections yielded a $Q_{II}$-Pn3m lattice constant of 282 ± 3 Å at 37.6°C. A rotating anode diffraction pattern obtained at 39°C from a sample of the same composition also detected a $Q_{II}$-Pn3m phase (data not shown). In all peptide-free and WALP-containing samples of DOPE-Me examined via synchrotron-source TRXRD, the first $Q_{II}$ phase to form was always $Q_{II}$-Pn3m. The first evidence of $Q_{II}$ phase formation in temperature-scan experiments was the appearance of the 110 and 111 peaks, as in the 37.0°C frame of Fig. 4 *A*. We defined $T_Q$ in the synchrotron source data as the temperature at which these reflections were first obviously resolved by eye, i.e., without the use of peak-fitting procedures. In practice, background subtraction and peak-fitting procedures could often identify traces of $Q_{II}$ phase diffraction at temperatures several tenths of a degree below the tabulated values of $T_Q$.

The values of $T_Q$ as determined via synchrotron-source and rotating anode TRXRD experiments are compared in Table 2. The values of $T_Q$ from the two methods generally agree with each other to within 0.2–2.4°. The $T_Q$ values for WALP19, WALP23, and WALP25 determined via this method are >2.4° lower than determined with the rotating anode apparatus. This is probably due to the greater sensitivity of the detector used at the synchrotron facility.

## Formation of $Q_{II}$-Ia3d phase in WALP/DOPE-Me systems

Synchrotron experiments showed that a second type of $Q_{II}$ phase, the $Q_{II}$-Ia3d phase, formed in addition to the $Q_{II}$-Pn3m phase in five compositions (Table 2). An example is given in Fig. 4 *B*, which shows diffraction patterns obtained at 0.5 mol % of WALP31 as it was ramped from 37.0 to 42.1°C at 1.5°C/h. The diffraction pattern obtained at 40.2°C shows the same four Pn3m reflections as in Fig. 4 *A*. At temperatures between ~40 and 41°C, there was an increase in diffracted intensity between the 110 and 111 reflections of the $Q_{II}$-Pn3m diffraction pattern. This resolved into a new peak at $q = 0.0427$ Å$^{-1}$ (160 Å), which became obvious at 41.3°C (*arrowhead*). The peak grew in intensity at higher temperatures, at the expense of the $Q_{II}$-Pn3m peaks. A peak at $q = 0.0503$ Å$^{-1}$ (125 Å) was also resolved in a pattern obtained 15 min after the end of the scan at 42.1°C. These two peaks are indicated by arrows, and index as the first two reflections (211 and 220) expected for a $Q_{II}$-Ia3d phase with a lattice constant of 354 Å. In the same pattern, there are new peaks at $q = 0.086$ Å$^{-1}$ and 0.127 Å$^{-1}$ (*arrowheads*). These peaks are too broad and contain too many candidate reflections to be accurately indexed. The peak at $q = 0.086$ Å$^{-1}$ may be a combination of the 332 reflection of the $Q_{II}$-Ia3d phase and reflections from the residual $Q_{II}$-Pn3m phase. The

**TABLE 2 $T_Q$ values and phases of WALP/DOPE-Me mixtures as determined by synchrotron- source and rotating-anode temperature-scan experiments**

| System | Peptide concentration (mol %) | $T_Q$ | | Final temperature (°C) | Phases present at final temperature in synchrotron-source experiment‡ |
|---|---|---|---|---|---|
| | | Synchrotron (°C)*† | Rotating-anode, (°C)* | | |
| Control | 0 | 59.4 | 59.7 | 61.9 | $L_\alpha/Q_{II}$-Pn3m |
| | 0 | 58.0 | 58.2 | 61.0 | $L_\alpha/Q_{II}$-Pn3m |
| WALP19 | 0.2 | <44.7 | 47.1 | 54.9 | $L_\alpha/Q_{II}$-Pn3m/$Q_{II}$-Ia3d/$H_{II}$ |
| | 0.5 | <33.0 | 34.8 | 42.6 | $L_\alpha/Q_{II}$-Ia3d/($H_{II}$) |
| WALP23 | 0.5 | <45.2 | 47.4 | 53.4 | $L_\alpha/Q_{II}$-Ia3d/($H_{II}$) |
| WALP25 | 0.5 | <49.6 | 52.0 | 59.8 | $L_\alpha/Q_{II}$-Pn3m/$Q_{II}$-Ia3d/$H_{II}$ |
| WALP27 | 0.2 | <54.0 | 54.2 | 62.8 | $Q_{II}$-Pn3m/$Q_{II}$-Im3m/$H_{II}$ |
| | 0.5 | 53.2 | 52.6 | 59.7 | $Q_{II}$-Pn3m/$H_{II}$ |
| WALP31 | 0.5 | 37.0 | 37.8 | 39.0 | $L_\alpha/Q_{II}$-Pn3m/$Q_{II}$-Ia3d |
| | 0.5 | 38.0 | 37.8 | 42.0 | $L_\alpha/Q_{II}$-Pn3m/$Q_{II}$-Ia3d |

*$T_Q$ measurements by both synchrotron and rotating-anode techniques were performed on samples from the same preparations, to remove the effect of preparation-to-preparation variability (see Materials and Methods). All measurements were made at a temperature scan rate of 1.5°C/h, except for the synchrotron experiment on 0.2 mol % WALP19, which was made at 2°C/h.

†< signifies that some $Q_{II}$ phase was present at the start of the temperature scan, which began at the temperature indicated.

‡The brackets in ($H_{II}$) signify that small amounts of $H_{II}$ phase were detected at the final temperature in the synchrotron experiments that did not appear in the corresponding rotating-anode experiments.

peak at $q = 0.127$ Å$^{-1}$ may represent high-order reflections from the $Q_{II}$-Ia3d phase.

In Fig. 4 *B*, the two reflections at $q = 0.042$ Å$^{-1}$ and 0.05 Å$^{-1}$ (observed at temperatures ≥41.3°C and 42.1°C, respectively) are too weak and too few in number to rigorously identify the new lattice. However, we tentatively identify this higher-temperature $Q_{II}$ lattice as the $Q_{II}$-Ia3d phase, based on the ratio of the apparent $Q_{II}$-Pn3m and $Q_{II}$-Ia3d lattice constants. Fig. 5 *A* shows plots of the lattice constants of the two $Q_{II}$ phases as a function of temperature for the experiment in Fig. 4 *B*. Fig. 5 *B* shows that the ratio of the $Q_{II}$-Ia3d and $Q_{II}$-Pn3m lattice constants over the entire temperature range is centered at 1.54, close to the value of 1.58 expected for coexisting $Q_{II}$-Ia3d and $Q_{II}$-Pn3m lattices (49,50). The putative $Q_{II}$-Ia3d phases were observed in synchrotron experiments at temperatures between 2° and 9°C above $T_Q$ in the WALP peptide systems (Table 2). The diffracted intensity from this phase grew at the expense of diffraction from the $Q_{II}$-Pn3m phase with increasing temperature.

$Q_{II}$-Ia3d phase formation is sensitive to the temperature history of the sample. The $Q_{II}$-Ia3d phase did not always appear in temperature-jump experiments using samples of the same composition that would form $Q_{II}$-Ia3d phase in temperature-scan experiments. The samples subjected to temperature-jump experiments were 0.5 mol % WALP19, 0.5 mol % WALP23, and 0.5 mol % WALP31 (data not shown). We do not know the reasons for this difference between temperature-scan and temperature-jump experiments.

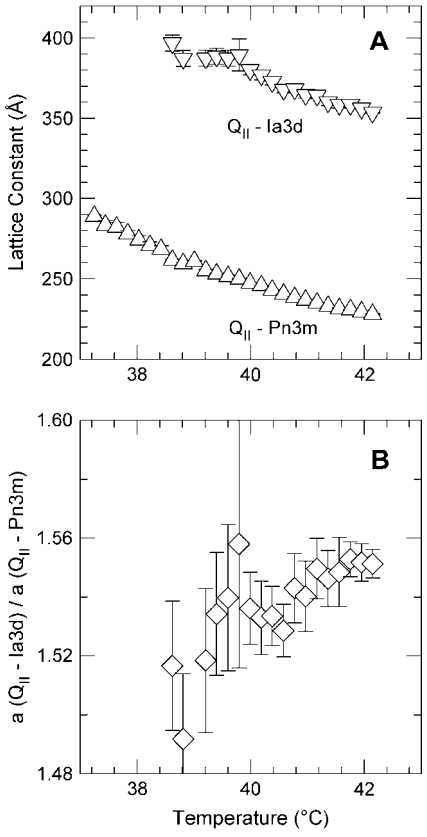


FIGURE 5 Lattice constants and lattice constant ratio of the $Q_{II}$ phases detected by the synchrotron TRXRD experiment in Fig. 4, as a function of temperature, for 0.5 mol % WALP31 in DOPE-Me. (*A*) Dependence of the lattice constants of the $Q_{II}$-Pn3m and $Q_{II}$-Ia3d phases on temperature. (*B*) Dependence of the ratio of the $Q_{II}$-Ia3d and $Q_{II}$-Pn3m lattice constants on temperature. This ratio is close to the value of 1.58 expected for coexisting $Q_{II}$-Ia3d and $Q_{II}$-Pn3m lattices (49,50).

## DISCUSSION

### Reduction in $T_Q$ and $T_H$ in DOPE-Me by WALP peptides

The principal result of this study is that WALP peptides substantially lower the temperatures at which $Q_{II}$ and $H_{II}$ phases form in DOPE-Me in a peptide-length-dependent manner (Figs. 2 and 3). For most peptides, the extent of the decrease in $T_Q$ and $T_H$ is linear in peptide concentration (Fig. 2). At constant peptide concentration, the extent to which each peptide reduces $T_Q$ and $T_H$ depends on the peptide length. This peptide length dependence is biphasic (Fig. 3): both the shortest (WALP19) and longest (WALP31) peptides were most effective in reducing the transition temperatures, compared to the peptides of intermediate lengths. Qualitatively, the phase behavior of WALP/DOPE-Me systems in temperature-scan experiments resembles that of pure DOPE-Me (28), where the $Q_{II}$ phase forms at a lower temperature than the $H_{II}$ phase, and $Q_{II}$-Pn3m is the first $Q_{II}$ phase to appear.

### Comparison with other studies of WALP effects on nonlamellar phase formation

Two recent studies investigated the effects of WALP peptides on nonlamellar phase transition temperatures in DOPE/DOPG (11) and in DEPE (10). In both reports, $Q_{II}$ phase formation was monitored primarily by observation of isotropic $^{31}$P NMR resonances, with x-ray diffraction used to demonstrate formation of the $Q_{II}$ phase under selected conditions. It should be noted that isotropic $^{31}$P NMR resonances can arise from interlamellar attachments 10–15° below $T_Q$ in lipids such as DOPE-Me (e.g., for DOPE-Me, $T_I$ in Ellens et al. (13) versus $T_Q$ in Cherezov et al. (28)).

Most of our results are consistent with those of Morein et al. (11) and van der Wel et al. (10). First, WALP peptides lower the temperatures at which isotropic resonances are observed in each lipid system. Second, both van der Wel et al. and Morein et al. found that in the series WALP19–WALP31, shorter peptides were more effective than longer peptides in inducing formation of the isotropic phase. We found that the shorter peptides in the series WALP19–WALP25 reduced $T_Q$ to a greater extent than did longer ones (Figs. 2 and 3). Third, van der Wel et al. (10) found that the shortest WALP peptides (WALP14 to WALP19) lowered the $T_H$ of DEPE, whereas WALP21 and WALP23 had

smaller or vanishing effects. In qualitative agreement with this, we found that the shortest peptide (WALP19) was most effective in reducing $T_H$ (Fig. 2). Finally, van der Wel et al. (10) found that 2 mol % of different-length WALP peptides had only a small effect (~1 Å or less) on the $H_{II}$ tube diameter in DEPE at 60°C. We found that the peptides had even smaller effects (<0.2 Å) on lattice dimensions in DOPE-Me at a concentration of 0.5 mol % (data not shown).

Nevertheless, there is one important difference in our results. In DOPE-Me, we observed that WALP31 reduced $T_Q$ to a significant extent. In contrast, in the studies by van der Wel and colleagues (10) and Morein et al. (11) it was found that WALP31 was less effective than shorter WALP peptides in inducing isotropic phase, perhaps due to a tendency of WALP31 to aggregate and phase-separate. In DOPE-Me, WALP31 does not phase-separate at concentrations up to 0.5 mol %; rather, it reduces $T_Q$ to an extent that is nearly linear in peptide concentration in the range 0.05–0.5 mol % (Fig. 3 *D*). Nevertheless, our data do suggest that WALP31 also has a tendency to oligomerize. The plot of $T_Q$ versus WALP31 concentration (Fig. 3 *D*) has a substantially larger apparent slope at concentrations <0.05 mol % than at higher concentrations. (We note a similar although less severe trend for WALP19 in Fig. 2 *A*.) Thus, at concentrations <0.05 mol % WALP31 appears to be present in a form that is more effective in reducing $T_Q$ on a mole-for-mole basis than at higher concentrations. This suggests that at concentrations >0.05 mol % WALP31 shows a higher tendency than shorter analogs to form dimers or small aggregates.

A likely explanation for the peptide-length dependence of the phase behavior is that WALP peptides that are too long or too short to fit into the bilayer will disturb lipid packing in DOPE-Me in different ways, but with a similar result at relatively low peptide concentrations: a lowering of both $T_Q$ and $T_H$.

In the case of the longer WALP31, the extent to which the system reacts by forming small aggregates of the peptide and cubic phases (as in DOPE-Me), versus more extensive aggregation and phase separation of the peptide (as in DEPE and PE/PG), seems to be very sensitive to the details of the particular system. The extent of hydrophobic mismatch should be comparable for a given WALP peptide in DOPE-Me ($L_\alpha$ phase bilayer thickness of 39 ± 5 Å; (46)), DOPE, DEPE, and DOPE/DOPG. It is therefore more likely that the differences in phase behavior of WALP31 in DOPE-Me as compared to the previous observations in DEPE and PE/PG are related to differences in the packing properties of the lipids in these systems. Since lipid packing is very different in the $Q_{II}$ and $H_{II}$ phases than in the $L_\alpha$ phase, it is interesting that $T_Q$ and $T_H$ are affected in the same way and to nearly the same extent by each peptide (Fig. 2). It may be that the peptides raise the free energy of the peptide-lipid $L_\alpha$ phase with respect to the pure lipid $L_\alpha$ phase more than they affect the free energy of the two inverted phases. This would have the effect of decreasing both $T_H$ and $T_Q$ in parallel as a function of peptide length, as is observed.

This explanation rationalizes most, but not all, of the data. Although $T_H$ and $T_Q$ are reduced by similar extents for all the peptides, the data in Fig. 2 show that $H_{II}$ phase exists for different peptide concentration ranges for different WALP peptides. $H_{II}$ phase is observed through 0.5 mol % for WALP27, but only through 0.2 mol % for WALP19 and WALP23, and only up until 0.05 mol % for WALP31. This could be due to nonequilibrium effects of the peptides on transition kinetics. However, different peptides may also be affecting the relative stability of $Q_{II}$ and $H_{II}$ phases differently. It has been pointed out that peptides could affect $Q_{II}$ phase stability more than $H_{II}$ phase stability if they change the monolayer Gaussian curvature elastic modulus of the lipids, $\kappa$ (16,51). Different-length peptides are expected to affect $\kappa$ differently, since this modulus is sensitive to the distribution of mass and intermolecular forces at different depths within the bilayer (52), and small changes in $\kappa$ have a big influence on $T_Q$ (16). Further studies of the effects of peptides on inverted phase stability (and especially on $Q_{II}$ phase stability) are required to settle this question.

It has been suggested that membrane-spanning peptides could change $T_H$ by effects on hydrophobic interstices (1) and $T_Q$ by stabilization of differences in membrane thickness within the unit cells of the inverted phases (53). Interstice stabilization cannot explain the observed effects on $T_Q$. $Q_{II}$ phases consist of continuous bilayers, with no hydrophobic interstices, so peptides cannot lower $T_Q$ by packing interstices. More recent theoretical work (54,55) indicates that the chain-stretching energy associated with the bilayer thickness gradient in the $Q_{II}$ phase is negligible for $Q_{II}$ phases with unit cells as large as those observed in this study. The difference in free energy with respect to the $L_\alpha$ phase is due to a difference in bending elastic and Gaussian curvature energy (54,55). Thus the WALP peptides do not change $T_Q$ via an effect on the chain-stretching energy of the $Q_{II}$ phase.

It is likely that WALP peptides change $T_H$ by stabilizing gradients in monolayer thickness in the $H_{II}$ phases (1). These gradients are imposed by the necessity of filling hydrophobic interstices between $H_{II}$ tubes. As discussed in Killian et al. (1), this could explain the effects of WALP peptides on $T_H$ for peptides that are shorter than the $L_\alpha$ phase bilayer thickness (WALP19, WALP23, and WALP25 in this system). It is not clear that this principle explains the effects of peptides that have helices longer than the $L_\alpha$ phase bilayer thickness (WALP27 and WALP31). If membrane-spanning peptides form rigid rods, they must exist only in the regions of the $H_{II}$ unit cell where the monolayers are opposed back-to-back, so that the two hydrophilic end groups of the peptide each reside in a lipid-water interface. These bilayer-like regions of the $H_{II}$ phase are thinner than the bilayers in the $L_\alpha$ phase bilayer from which the $H_{II}$ phase forms. Thus, there would be an increased extent of peptide-lipid length mismatch in the $H_{II}$ versus the $L_\alpha$ phase for peptides like WALP27 and WALP31. This would increase $T_H$, rather than lower it, as we observed (Fig. 3, *C* and *D*). However, such

''long'' membrane-spanning peptides might be able to lower $T_H$ by filling hydrophobic interstices directly, if they can form kinks or bends. If the end groups of the peptide have to be in lipid-water interfaces, simple geometry shows that the peptide can fill an interstice if it can bend or kink in the middle by ~30°. This might explain the efficacy of ''long'' peptides in reducing $T_H$. Interestingly, in peptides mimicking the membrane-spanning domains of some fusion-mediating proteins, activity in fusing pure lipid vesicles is correlated with increasing conformational flexibility of the peptides (30–33). Membrane fusion intermediates contain hydrophobic interstices (14,56). It may be that the more flexible peptides have the ability to form kinks, and act in part by filling the hydrophobic interstices within fusion intermediates in an analogous manner.

In addition to WALP peptides, other length-mismatched, transmembrane peptides can also influence lipid phase behavior. Recently, Liu et al. (12) studied the effects of peptides with polyleucine membrane-spanning domains and positively charged flanking residues on the $T_H$ of DEPE and dipalmitelaidoylphosphatidylethanolamine, and inferred the presence of $Q_{II}$ phases from $^{31}P$ NMR data. In these experiments, transmembrane peptides longer than the PE membrane thickness also lowered $T_H$ more than peptides with lengths approximately the same as the lipid membrane thickness. The results are very similar to our results comparing the effects of WALP31 versus shorter analogs on $T_H$ and $T_Q$.

## Implications for protein-mediated membrane fusion: influence of transmembrane domains

### *Proximity of biomembrane systems to the lamellar/nonlamellar phase boundary*

Many biomembranes or biomembrane lipid extracts form nonlamellar phases if incubated above the physiological temperature (see, e.g., de Grip et al. (57), Burnell et al. (58), Gounaris et al. (59), Ranck et al. (60), Quinn et al. (61), and Lindblom et al. (62)), if dehydrated (see, e.g., Gruner et al. (63), Crowe and Crowe (65), and Gordon-Kamm and Steponkus (65)), or if treated with divalent cations (see, e.g., Cullis et al. (66), Albert et al. (67), Nicolay et al. (68), and Killian et al. (69)). Furthermore, the fusion rate in several lipid systems accelerates as one approaches the $L_\alpha/Q_{II}$ phase boundary, and the intermediates in membrane fusion correspond to intermediates in this phase transition. In some lipid extracts, $Q_{II}$ phases or $Q_{II}$ phase precursors are observed (62). More generally, $Q_{II}$ phases should be stable in phospholipids in a broad temperature interval below $T_H$, although $Q_{II}$ phase formation can be slowed or inhibited in some cases (14). $Q_{II}$ phases even form in mixtures of unsaturated acyl-chain PC and cholesterol; two plasma membrane lipid components that cannot form inverted phases in excess water by themselves ((70,71); B. Tenchov, R. C. MacDonald, and D. P. Siegel, unpublished). Under physiological conditions, the lipids of many biomembranes may be near the lamellar/$Q_{II}$ phase boundary. Addition of agents such as WALP-like transmembrane peptides that lower $T_Q$ could therefore increase the tendency of the lipids to form fusion pore structures ($Q_{II}$ phase precursors) between apposed membranes.

### *The transmembrane domains of proteins may facilitate membrane fusion*

The membrane-spanning domains of viral fusion proteins appear to act by stabilizing nascent fusion pores at a post-hemifusion stage (see, e.g., Kemble et al. (72), Chernomordik et al. (73), Melikyan et al. (74), Razinkov et al. (75), Markosyan et al. (76), Melikyan et al. (77), Armstrong et al. (78), and Frolov et al. (79); for reviews, see Schroth-Diez et al. (29) and Earp et al. (80)). Moreover, peptides corresponding to the transmembrane domains of fusion-mediating proteins have been shown to induce liposome fusion in the absence of other peptides or proteins (30–33). The peptides in these studies acted at a posthemifusion stage, consistent with peptide action in stabilizing nascent fusion pores. In addition, peptides corresponding to mutants with reduced fusion activity in vivo were less active in stimulating fusion than the wild-type sequences.

In agreement with these results, this work also indicates that transmembrane peptides should increase the susceptibility of the lipids of membranes to membrane fusion. The peptides do so through an effect on the lipid phase behavior. Changes in lipid-peptide composition that stabilize $Q_{II}$ phases relative to the $L_\alpha$ phase also stabilize fusion pores (16). We have shown that transmembrane WALP peptides substantially stabilize $Q_{II}$ phases (lower $T_Q$) at concentrations of only 0.5 mol %, which is comparable to physiological conditions. For example, the fusion-mediating protein influenza hemagglutinin (HA) is present at a monomer concentration of 1.5 mol %, with each monomer having a single transmembrane domain (calculated using data from (81)). Transmembrane domains, if they have effects similar to those of WALP peptides on $T_Q$, could substantially accelerate fusion pore formation in biomembranes by a direct effect on the lipids. This is in addition to, or instead of, action of the domains through interactions with other regions of the fusion proteins. Our results indicate that domains that are either substantially longer or shorter than the thickness of the lipid bilayer should be especially effective (Table 1and Fig. 3). If the membrane-spanning domains of fusion proteins are as effective as WALP19 in reducing $T_Q$ in DOPE-Me, it can be shown that a local concentration 1.0 mol % of such domains would lower the energy of fusion pores by ~40 $k_BT$ (using data for DOPE-Me (16)).

The sequences of membrane-spanning domains affect their fusion activity, both in full-length proteins in vivo and in peptides in model membranes. For example, Langosch

et al. (30,31), Hofman et al. (33), and Dennison et al. (32) infer that facile interconversion between $\alpha$-helical and $\beta$-sheet structure is important for optimal fusion activity. It would be interesting to test the effects of different fusion protein membrane-spanning domains on $T_Q$. This would permit us to infer what (if any) role the $Q_{II}$-phase stabilizing effect plays in activity of these domains, and whether the observed differences in activity among domains of different sequences is due to differences in the degree of $Q_{II}$ phase stabilization, or to other effects, such as changes in interactions with other domains of the fusion proteins, or differences in the ability to stabilize hydrophobic interstices.

### *How much do the transmembrane domains of fusion proteins resemble WALP peptides?*

The transmembrane domain of at least one fusion protein, influenza HA, has some features in common with the WALP peptides. The HA membrane-spanning domain has interfacial anchoring groups similar to those in WALP peptides, although fewer in number. In 18 strains of influenza virus, all had at least one aromatic amino acid residue in a six-residue-wide band at the N-terminal end of the domain (seven strains had two), and 16 had either a tryptophan or phenylalanine group at a single conserved location at the C-terminal end (40). The aromatic residues in these sequences could act as interfacial anchors (82), as do pairs of tryptophan residues in the WALP peptides (5). The length of the sequence between and including the inferred interfacial anchors in the HA transmembrane domains is ~19–21 residues, as in a WALP peptide with a total length of 23–25 residues. WALP23 has a substantial effect on $T_Q$ (15°C/mol %) of DOPE-Me (Figs. 2 *B* and 3). Thus, it is possible that the transmembrane domain of HA exerts an influence on $T_Q$ in biomembranes that is analogous to the effect of WALP peptides in DOPE-Me.

We are grateful for the expert assistance of Dr. Malcolm S. Capel (National Synchrotron Light Source, Beamline X12B) in collecting the synchrotron TRXRD data. This project was supported in part by grants from the National Institutes of Health (DK36849, DK46295, RR15569, GM34968, and GM61070), the National Science Foundation (DIR9016683), and Science Foundation Ireland (02-IN1-B266).

## REFERENCES

1. Killian, J. A., I. Salemink, M. R. R. de Planque, G. Lindblom, R. E. Koeppe II, and D. V. Greathouse. 1996. Induction of nonbilayer structures in diacylphosphatidylcholine model membranes by transmembrane $\alpha$-helical peptides: Importance of hydrophobic mismatch and proposed role of tryptophans. *Biochemistry.* 35:1037–1045.
2. Morein, S., E. Strandberg, J. A. Killian, S. Persson, G. Avidson, R. E. Koeppe II, and G. Lindblom. 1997. Influence of membrane-spanning $\alpha$-helical peptides on the phase behavior of the dioleoylphosphatidylcholine/water system. *Biophys. J.* 73:3078–3088.
3. de Planque, M. R. R., J. A. Kruijtzer, R. M. J. Liskamp, D. Marsh, D. V. Greathouse, R. E. Koeppe II, B. de Kruijff, and J. A. Killian. 1999. Different membrane anchoring positions of tryptophan and lysine in synthetic transmembrane $\alpha$-helical peptides. *J. Biol. Chem.* 274: 20839–20846.
4. de Planque, M. R. R., E. Goormaghtigh, D. V. Greathouse, R. E. Koeppe II, J. A. W. Kruijtzer, R. M. J. Liskamp, B. de Kruijff, and J. A. Killian. 2001. Sensitivity of single membrane-spanning $\alpha$-helical peptides to hydrophobic mismatch with a lipid bilayer: effects on backbone structure, orientation, and extent of membrane incorporation. *Biochemistry.* 40:5000–5010.
5. de Planque, M. R. R., J. A. A. Demmers, B. B. Bonev, R. E. Koeppe II, D. V. Greathouse, F. Separovic, A. Watts, and J. A. Killian. 2003. Interfacial anchor properties of tryptophan residues in transmembrane peptides can dominate over hydrophobic mismatch effects in peptide-lipid interactions. *Biochemistry.* 42:5341–5348.
6. Van der Wel, P. C. A., E. Strandberg, J. A. Killian, and R. E. Koeppe II. 2002. Geometry and intrinsic tilt of a tryptophan-anchored transmembrane $\alpha$-helix determined using $^2$H NMR. *Biophys. J.* 83: 1479–1488.
7. Weiss, T. M., P. C. A. van der Wel, J. A. Killian, R. E. Koeppe II, and H. W. Huang. 2003. Hydrophobic mismatch between helices and lipid bilayers. *Biophys. J.* 84:379–385.
8. Strandberg, E., S. Ozdirekcan, D. T. S. Rijkers, P. C. A. van der Wel, R. E. Koeppe II, and J. A. Killian. 2004. Tilt angle of transmembrane model peptides in oriented and non-oriented lipid bilayers as determined by $^2$H solid-state NMR. *Biophys. J.* 86:3709–3721.
9. Demmers, J. A. A., E. van Duijn, J. Haverkamp, D. V. Greathouse, R. E. Koeppe II, A. J. R. Heck, and J. A. Killian. 2001. Interfacial positioning and stability of transmembrane peptides in lipid bilayers as studied by hydrogen/deuterium exchange and mass spectrometry. *J. Biol. Chem.* 276:34501–34508.
10. van der Wel, P. C. A., T. Pott, S. Morein, D. V. Greathouse, R. E. Koeppe II, and J. A. Killian. 2000. Tryptophan-anchored transmembrane peptides promote formation of nonlamellar phase in phosphatidylethanolamine model membranes in a mismatch-dependent manner. *Biochemistry.* 39:3124–3133.
11. Morein, S., R. E. Koeppe II, G. Lindblom, B. de Kruijff, and J. A. Killian. 2000. The effect of peptide/lipid hydrophobic mismatch on the phase behavior of model membranes mimicking the lipid composition of *Escherichia coli* membranes. *Biophys. J.* 78:2475–2485.
12. Liu, F., R. N. A. H. Lewis, R. S. Hodges, and R. N. McElhaney. 2001. A differential scanning calorimetric and $^{31}$P NMR spectroscopic study of the effect of transmembrane peptides on the lamellar-reversed hexagonal phase transition of phosphatidylethanolamine model membranes. *Biochemistry.* 40:760–768.
13. Ellens, H., D. P. Siegel, D. Alford, P. L. Yeagle, L. Boni, L. J. Lis, P. J. Quinn, and J. Bentz. 1989. Membrane fusion and inverted phases. *Biochemistry.* 28:285–294.
14. Siegel, D. P. 1999. The modified stalk mechanism of lamellar/inverted phase transitions and its implications for membrane fusion. *Biophys. J.* 76:292–313.
15. Epand, R. M. 1998. Lipid polymorphism and protein-lipid interactions. *Biochim. Biophys. Acta.* 1376:353–368.
16. Siegel, D. P., and M. M. Kozlov. 2004. The Gaussian curvature elastic modulus of N-monomethylated dioleoylphosphatidylethanolamine: relevance to membrane fusion and lipid phase behavior. *Biophys. J.* 87:366–374.
17. Siegel, D. P., J. L. Burns, M. H. Chestnut, and Y. Talmon. 1989. Intermediates in membrane fusion and bilayer/non-bilayer phase transitions imaged by time-resolved cryo-transmission electron microscopy. *Biophys. J.* 56:161–169.
18. Siegel, D. P., W. J. Green, and Y. Talmon. 1994. The mechanism of lamellar-to-inverted hexagonal phase transitions: a study using temperature-jump cryo-electron microscopy. *Biophys. J.* 66:402–414.
19. Frederik, P. M., K. N. J. Burger, M. C. A. Stuart, and A. J. Verkleij. 1991. Lipid polymorphism as observed by cryo-electron microscopy. *Biochim. Biophys. Acta.* 1062:133–141.
20. Siegel, D. P. 1986. Inverted micellar intermediates and the transitions between lamellar, inverted hexagonal, and cubic lipid phases. III.

Formation of isotropic and inverted cubic phases and fusion via intermediates in transitions between $L_\alpha$ and $H_{II}$ phases. *Chem. Phys. Lipids*. 42:279–301.

21. Siegel, D. P., and J. L. Banschbach. 1990. Lamellar/inverted cubic ($L_\alpha$/$Q_{II}$) phase transition in N-methylated dioleoylphosphatidylethanolamine. *Biochemistry*. 29:5975–5981.
22. Yeagle, P. L., R. M. Epand, C. D. Richardson, and T. D. Flanagan. 1991. Effects of the 'fusion peptide' from measles virus on the structure of N-methyl dioleoylphosphatidylethanolamine membranes and their fusion with Sendai virus. *Biochim. Biophys. Acta*. 1065: 49–53.
23. Epand, R. M., and R. F. Epand. 1994. Relationship between the infectivity of influenza virus and the ability of its fusion peptide to perturb bilayers. *Biochem. Biophys. Res. Commun*. 202:1420–1425.
24. Epand, R. F., I. Martin, J. M. Ruysschaert, and R. M. Epand. 1994. Membrane orientation of the SIV fusion peptide determines its effect on bilayer stability and ability to promote membrane fusion. *Biochem. Biophys. Res. Commun*. 205:1938–1943.
25. Nieva, J. L., A. Alonso, G. Basáñez, F. M. Goñi, A. Gulik, R. Vargas, and V. Luzzati. 1995. Topological properties of two cubic phases of a phospholipid:cholesterol:diacylglycerol aqueous system and their possible implications in the phospholipase C-induced liposome fusion. *FEBS Lett*. 368:143–147.
26. Davies, S. M. A., R. F. Epand, J. P. Bradshaw, and R. M. Epand. 1998. Modulation of lipid polymorphism by the feline leukemia virus fusion peptide: implications for the fusion mechanism. *Biochemistry*. 37:5720–5729.
27. Basáñez, G., F. M. Gõni, and A. Alonso. 1998. Effect of single chain lipids on phospholipase C-promoted membrane fusion. A test for the stalk hypothesis of membrane fusion. *Biochemistry*. 37:3901–3908.
28. Cherezov, V. C., D. P. Siegel, W. Shaw, S. W. Burgess, and M. Caffrey. 2003. The kinetics of non-lamellar phase formation in DOPE-Me: Relevance to biomembrane fusion. *J. Membr. Biol*. 195:165–182.
29. Schroth-Diez, B., K. Ludwig, B. Baljinnyam, C. Kozerski, Q. Huang, and A. Hemrann. 2000. The role of the transmembrane and of the intraviral domain of glycoproteins in membrane fusion *f*o enveloped viruses. *Biosci. Rep*. 20:571–595.
30. Langosch, D., B. Brosig, and R. Pipkorn. 2001. Peptide mimetics of the vesicular stomatitis virus G-protein transmembrane segment drive membrane fusion in vitro. *J. Biol. Chem*. 276:32016–32021.
31. Langosch, D., J. M. Crane, B. Brosig, A. Hellwig, L. K. Tamm, and J. Reed. 2001. Peptide mimetics of SNARE transmembrane segments drive membrane fusion depending on their conformational plasticity. *J. Mol. Biol*. 311:709–721.
32. Dennison, S. M., N. Greenfield, J. Lenard, and B. R. Lentz. 2002. VSV transmembrane domain (TMD) peptide promotes PEG-mediated fusion of liposomes in a conformationally sensitive fashion. *Biochemistry*. 41:14925–14934.
33. Hofman, M. W., K. Weise, J. Ollesch, P. Agrawal, H. Stalz, W. Stelzer, F. Hulsbergen, H. de Groot, K. Gerwert, J. Reed, and D. Langosch. 2004. De novo design of conformationally flexible transmembrane peptides driving membrane fusion. *Proc. Natl. Acad. Sci. USA*. 101:14776–14781.
34. Tsurudome, M., R. Glück, R. Graf, R. Falchetto, U. Schaller, and J. Brunner. 1992. Lipid interactions of the hemagglutinin HA2 $NH_2$-terminal segment during influenza virus-induced membrane fusion. *J. Biol. Chem*. 267:20225–20232.
35. Lear, J. D., and W. F. DeGrado. 1987. Membrane binding and conformational properties of peptides representing the $HN_2$ terminus of influenza HA-2. *J. Biol. Chem*. 262:6500–6505.
36. Nieva, J. L., and A. Agirre. 2003. Are fusion peptides a good model to study viral cell fusion? *Biochim. Biophys. Acta*. 1614:104–115.
37. Tamm, L. K., X. Han, Y. Li, and A. L. Lai. 2002. Structure and function of membrane fusion peptides. *Biopolymers*. 66:249–260.
38. Tamm, L. K., and X. Han. 2000. Viral fusion peptides: a tool set to disrupt and connect biological membranes. *Biosci. Rep*. 20: 501–518.
39. Martin, I., J.-M. Ruysschaert, and R. M. Epand. 1999. Role of the N-terminal peptides of viral envelope proteins in membrane fusion. *Adv. Drug Deliv. Rev*. 38:233–255.
40. Tatulian, S. A., and L. K. Tamm. 2000. Secondary structure, oligomerization, and lipid interactions of the transmembrane domain of influenza hemagglutinin. *Biochemistry*. 39:496–507.
41. Caffrey, M. 1989. The study of lipid phase transition kinetics by time-resolved x-ray diffraction. *Annu. Rev. Biophys. Biophys. Chem*. 18:159–186.
42. Greathouse, D. V., R. L. Goforth, T. Crawford, and P. C. A. van der Wel. 2001. Optimized aminolysis conditions for cleavage of N-protected hydrophobic peptides from solid-phase resins. *J. Pept. Res*. 57:519–527.
43. Blanton, T. N., T. C. Huang, H. Toroya, C. R. Hubbard, S. B. Robie, D. Louer, H. E. Gobel, G. Will, R. Gilles, and T. Rafferty. 1995. JCPDS – International centre for diffraction data study of silver behenate. A possible low-angle X-ray diffraction calibration standard. *Powder Diffraction*. 10:91–95.
44. Cheng, A., and M. Caffrey. 1996. Free radical mediated x-ray damage of model membranes. *Biophys. J*. 70:2212–2222.
45. Cherezov, V. C., A. Cheng, J.-M. Peit, O. Diat, and M. Caffrey. 2000. Biophysics and synchrotron radiation. Where the marriage fails. X-ray damage of lipid membranes and mesophases. *Cell. Mol. Biol*. 46:1133–1145.
46. Gruner, S. M., M. W. Tate, G. L. Kirk, P. T. C. So, D. C. Turner, D. T. Keane, C. P. S. Tilcock, and P. R. Cullis. 1988. X-ray diffraction study of the polymorphic behavior of N-methylated dioleoylphosphatidylethanolamine. *Biochemistry*. 27:2853–2866.
47. Longley, W., and T. J. McIntosh. 1983. A bicontinuous tetrahedral structure in a liquid-crystalline lipid. *Nature*. 303:612–614.
48. Harper, P. E., S. M. Gruner, R. N. A. H. Lewis, and R. N. McElhaney. 2000. Electron density modeling and reconstruction of infinite periodic minimal surfaces (IPMS) based phases in lipid-water systems. II. Reconstruction of D surface based phases. *Eur. Phys. J. E*. 2: 229–245.
49. Hyde, S., S. Andersson, B. Ericsson, and K. Larsson. 1984. A cubic structure consisting of a lipid bilayer forming an infinite periodic minimum surface of the gyroid type in the glyceromonooleate-water system. *Z. Krystallogr*. 168:213–219.
50. Andersson, S., S. T. Hyde, K. Larsson, and S. Lidin. 1988. Minimal surfaces and structures: from inorganic and metal crystals to cell membranes and biopolymers. *Chem. Rev*. 88:221–242.
51. Siegel, D. P. 2005. The relationship between bicontinuous inverted cubic phases and membrane fusion. *In* Bicontinuous Structured Liquid Crystals. M. L. Lynch and P. T. Spicer, editors. Marcel Dekker, New York, 59–98.
52. Seddon, J. M. 1990. Structure of the inverted hexagonal ($H_{II}$) phase, and non-lamellar phase transitions of lipids. *Biochim. Biophys. Acta*. 1031:1–69.
53. de Planque, M. R. R., and J. A. Killian. 2003. Protein-lipid interactions studied with designed transmembrane peptides: role of hydrophobic mis-matching and interfacial anchoring. *Mol. Membr. Biol*. 20: 271–284.
54. Templer, R. H., B. J. Khoo, and J. M. Seddon. 1998. Gaussian curvature modulus of an amphiphilic monolayer. *Langmuir*. 14: 7427–7434.
55. Schwarz, U., and G. Gompper. 2002. Bicontinuous surfaces in self-assembling amphiphilic systems. *In* Morphology of Condensed Matter. Lecture Notes in Physics, Vol. 600. K. Mecke and D. Stoyan, editors. Springer-Verlag, New York. 107–151.
56. Siegel, D. P. 2005. Lipid membrane fusion. *In* The Structure of Biological Membranes. P. L. Yeagle, editor. CRC Press, Boca Raton, FL. 255–308.
57. de Grip, W. J., E. H. S. Drenthe, C. J. A. van Echteld, B. de Kruijff, and A. J. Verkleij. 1979. A possible role of rhodopsin in maintaining bilayer structure in the photoreceptor membrane. *Biochim. Biophys. Acta*. 558:330–337.

58. Burnell, E., L. van Alphen, A. Verkleij, and B. de Kruijff. 1980. $^{31}$P nuclear magnetic resonance and freeze-fracture electron microscopy studies of *Escherichia coli*. *Biochim. Biophys. Acta.* 597:492–501.

59. Gounaris, K., D. A. Mannock, A. Sen, A. P. R. Brain, W. P. Williams, and P. J. Quinn. 1983. Polyunsaturated fatty acyl residues of galactolipids are involved in the control of bilayer/non-bilayer lipid transitions in higher plant chloroplasts. *Biochim. Biophys. Acta.* 732:229–242.

60. Ranck, J. L., L. Letellier, E. Shechter, B. Krop, P. Pernot, and A. Tardieu. 1984. X-ray analysis of the kinetics of *Escherichia coli* lipid and membrane structural transitions. *Biochemistry.* 23:4955–4961.

61. Quinn, P. J., A. P. R. Brain, L. C. Stewart, and M. Kates. 1986. The structure of membrane lipids of the extreme halophile, *Halobacterium cutirubrum*, in aqueous systems studied by freeze-fracture. *Biochim. Biophys. Acta.* 863:213–223.

62. Lindblom, G., I. Brentel, M. Sjolund, G. Wikander, and A. Wieslander. 1986. Phase behavior of membrane lipids from *Acholeplasma laidlawii*: importance of a single lipid forming nonlamellar phases. *Biochemistry.* 25:7502–7510.

63. Gruner, S. M., K. J. Rothschild, and N. A. Clark. 1982. X-ray diffraction and electron microscope study of phase separation in rod outer segment photoreceptor membrane multilayers. *Biophys. J.* 39: 241–251.

64. Crowe, L. M., and J. H. Crowe. 1982. Hydration-dependent hexagonal phase lipid in a biological membrane. *Arch. Biochem. Biophys.* 217:582–587.

65. Gordon-Kamm, W. J., and P. L. Steponkus. 1984. Lamellar-to-hexagonal$_{II}$ phase transitions in the plasma membrane of isolated protoplasts after freeze-induced dehydration. *Proc. Natl. Acad. Sci. USA.* 81:6373–6377.

66. Cullis, P. R., B. de Kruijff, M. J. Hope, R. Nayar, A. Rietveld, and A. J. Verkleij. 1980. Structural properties of phospholipids in the rat liver inner mitochondrial membrane. A $^{31}$P NMR study. *Biochim. Biophys. Acta.* 600:625–635.

67. Albert, A. D., A. Sen, and P. L. Yeagle. 1984. The effect of calcium on the bilayer stability of lipids from bovine rod outer segment disk membranes. *Biochim. Biophys. Acta.* 771:28–34.

68. Nicolay, K., R. van der Neut, J. J. Fok, and B. de Kruijff. 1985. Effects of adriamycin on lipid polymorphism in cardiolipin-containing model and mitochondrial membranes. *Biochim. Biophys. Acta.* 819:55–65.

69. Killian, J. A., M. C. Koorengevel, J. A. Bouwstra, G. Gooris, W. Dowhan, and B. de Kruijff. 1994. Effect of divalent cations on lipid organization of cardiolipin isolated from *Escherichia coli* strain AH930. *Biochim. Biophys. Acta.* 1189:225–232.

70. Epand, R. M., D. W. Hughes, B. G. Sayer, N. Borochov, D. Bach, and E. Wachtel. 2003. Novel properties of cholesterol-dioleoylphosphatidylcholine mixtures. *Biochim. Biophys. Acta.* 1616:196–208.

71. Epand, R. M., R. F. Epand, A. D. Bain, B. G. Sayer, and D. W. Hughes. 2004. Properties of polyunsaturated phosphatidylcholine membranes in the presence and absence of cholesterol. *Magn. Reson. Chem.* 42:139–147.

72. Kemble, G. W., T. Danieli, and J. M. White. 1994. Lipid-anchored influenza hemagglutinin promotes hemifusion, not complete fusion. *Cell.* 76:383–391.

73. Chernomordik, L. V., L. Eugenia, M. M. Kozlov, V. A. Frolov, and J. Zimmerberg. 1999. Structural intermediates in influenza hemagglutinin-mediated fusion. *Mol. Membr. Biol.* 16:33–42.

74. Melikyan, G. B., S. Lin, M. G. Roth, and F. S. Cohen. 1999. Amino acid sequence requirements of the transmembrane and cytoplasmic domains of influenza virus hemagglutinin fro viable membrane fusion. *Mol. Biol. Cell.* 10:1821–1836.

75. Razinkov, V. I., G. B. Melikyan, and F. S. Cohen. 1999. Hemifusion between cells expressing hemagglutinin of influenza virus and planar membranes can precede the formation of fusion pores that subsequently fully enlarge. *Biophys. J.* 77:3144–3151.

76. Markosyan, R. M., F. S. Cohen, and G. B. Melikyan. 2000. The lipid-anchored ectodomain of influenza virus hemagglutinin (GPI-HA) is capable of inducing nonenlarging fusion pores. *Mol. Biol. Cell.* 11:1143–1152.

77. Melikyan, G. B., R. K. Markosyan, M. G. Roth, and F. S. Cohen. 2000. A point mutation in the transmembrane domain of hemagglutinin of influenza hemagglutinin stabilizes a hemifusion intermediate that can transit to fusion. *Mol. Biol. Cell.* 11:3765–3775.

78. Armstrong, R. T., A. S. Kushnir, and J. M. White. 2000. The transmembrane domain of influenza hemagglutinin exhibits a stringent length requirement to support the hemifusion to fusion transition. *J. Cell Biol.* 151:425–437.

79. Frolov, V. A., M. S. Cho, P. Bronk, T. S. Reese, and J. Zimmerberg. 2000. Multiple local contact sites are induced by GPI-linked influenza hemagglutinin during hemifusion and flickering pore formation. *Traffic.* 1:622–630.

80. Earp, L. J., S. E. Delos, H. E. Park, and J. M. White. 2004. The many mechanisms of viral membrane fusion proteins. *Curr. Top. Microbiol. Immunol.* 285:25–66.

81. Lamb, R. A., and R. M. Krug. 1996. Orthomyxoviridae: the viruses and their replication. *In* Virology, Vol. 1. B. N. Fields, D. M. Knirpe, and P. M. Howley, editors. Lippincott-Raven, Philadelphia. 1353–1395.

82. Wimley, W. C., and S. H. White. 1996. Experimentally determined hydrophobicity scale for proteins at membrane interfaces. *Nature. Struct. Biol.* 3:842–848.